

NONLINEAR OPTICAL PHENOMENA

PACS numbers: 42.70.Mp; 42.65 Dr; 42.55.Ye

Stimulated Raman scattering in alkaline-earth tungstate crystals

P G Zverev, T T Basiev, A A Sobol', V V Skornyakov, L I Ivleva, N M Polozkov, V V Osiko

DOI: 10.1070/QE2000v030n01ABEH001658

Abstract. Results on spontaneous Raman spectroscopy of alkaline-earth tungstate crystals are presented. The frequency of the modes active in stimulated Raman scattering (SRS) modes was found to increase and their width to decrease with increasing cation radius and mass in the series of alkaline-earth (Ca, Sr, Ba) tungstates. High peak values of the Raman scattering cross section for barium and strontium tungstate crystals — new media offering promise for SRS — were predicted and observed in the experiments. Laser experiments on the SRS threshold showed that the SRS gain for the barium tungstate crystal was close to the record value observed for the barium nitrate crystal, which is extensively used in SRS.

1. Introduction

The search for new efficient nonlinear solid-state materials for SRS and their study is an important task in laser physics because of the need for laser radiation sources operating in new spectral regions. Tungstate crystals represent one of the most promising classes of SRS-active media. The first observation of SRS in a $CaWO_4$ crystal was reported in Ref. [1]. However, this crystal has not found extensive application in practice because of its low SRS gain. In 1985, a 'double' potassium – gadolinium tungstate crystal $KGd(WO_4)_2$ has been first proposed as an SRS-active material [2, 3]. The $KGd(WO_4)_2$ crystal has an anisotropic structure and, therefore, one can excite SRS in it with frequency shifts of 901 and 767 cm^{-1}, depending on the direction of propagation and polarisation of radiation [2]. At both frequencies, the SRS gain at the wavelength of 1064 nm is about 6 cm GW^{-1}, which is a factor of 1.8 lower than the value for the $Ba(NO_3)_2$ crystal [4], which is known for its record SRS gain.

The crystal structure of tungstate crystals makes it possible to introduce impurity ions and use these crystals as matrices for laser active elements with nonlinear SRS self-conversion of radiation to a new spectral range [5]. Our aim will be to search for alkaline-earth tungstate crystals with the highest SRS efficiency.

P G Zverev, T T Basiev, A A Sobol', V V Skornyakov, L I Ivleva, N M Polozkov, V V Osiko Laser Materials and Technology Research Centre, Institute of General Physics, Russian Academy of Sciences, ul. Vavilova 38, 117942 Moscow, Russia,
tel/fax +7(095) 135 02 67, e-mail: basiev@lst.gpi.ru

Received 19 August 1999
Kvantovaya Elektronika **30** (1) 55 – 59 (2000)
Translated by A Kirkin, edited by L Dwivedi

2. Spectroscopic study of tungstate crystals

As shown in Ref. [6], a study of an SRS-active mode of a medium by spontaneous Raman spectroscopy and, in particular, measurement of the peak and integrated scattering cross sections makes it possible to compare different materials and predict their SRS properties. $MeWO_4$ alkaline-earth tungstate crystals (Me = Ca, Sr, Ba is an alkaline-earth metal) were studied with spectroscopic apparatus described in detail in [6]. The radiation source was an argon laser oscillating at the wavelength of 488 nm. The laser radiation power reaching a crystal was ~ 1 W. The spontaneous Raman spectrum was recorded in the backscattering direction with a SPEX Ramalog-1403 spectrometer. The spectral resolution of the apparatus reached 0.2 cm^{-1}. The peak and integrated cross sections were normalised to the scattering cross section measured for a diamond crystal 0.8 mm thick.

We studied objects in the form of single-crystal and polycrystalline samples. Single-crystal $BaWO_4$ boules of high optical quality were grown by Czochralski method in air from a platinum crucible using a standard Kristall-3M unit. A seed crystal was oriented at 90° to the fourth-order axis. Crystals grown in this way were of ellipsoidal shape. The boules were up to 70 mm long and about 15 mm in diameter. The $CaWO_4$ single crystals were grown in air from platinum – rhodium crucibles. In our preliminary studies, we synthesised polycrystalline $CaWO_4$, $SrWO_4$, and $BaWO_4$ samples by sintering a mixture of the corresponding carbonate $CaCO_3$, $SrCO_3$, or $BaCO_3$ and tungsten oxide WO_3 in an oven at a temperature of 1100 – 1200 °C during 30 – 40 h. In measurements of the scattering cross sections, we used single-crystal plates 0.8 mm thick.

The spontaneous Raman spectra of $MeWO_4$ tungstates with increasing cation radius in the $Ca^{2+} \rightarrow Sr^{2+} \rightarrow Ba^{2+}$ series are presented in Fig. 1. One can see that each of them has the strongest narrow line in a spectral region of 910 – 925 cm^{-1}, which corresponds to the internal symmetric valence vibration A_{1g} in the tetrahedral group WO_4. Table 1 lists the Raman frequencies Ω_R and the spectral widths $\Delta\Omega_R$ of the A_{1g} mode in these crystals at temperatures of 300 K and 77 K, and the maximum frequency of lattice vibrations of the crystal matrix ω_{lat}^{max}. One can see from Table 1 that an increase of the cation radius and mass in the $Ca^{2+} \rightarrow Sr^{2+} \rightarrow Ba^{2+}$ series leads to an increase in the energy and reduction in the width of the high-frequency A_{1g} mode and correlates with a reduction in the maximum frequency of the lattice vibrations.

The $CaWO_4$ crystal was found to have a specific feature, namely, an asymmetric scattering spectrum of the SRS-active mode, indicating the presence of two closely spaced spectral

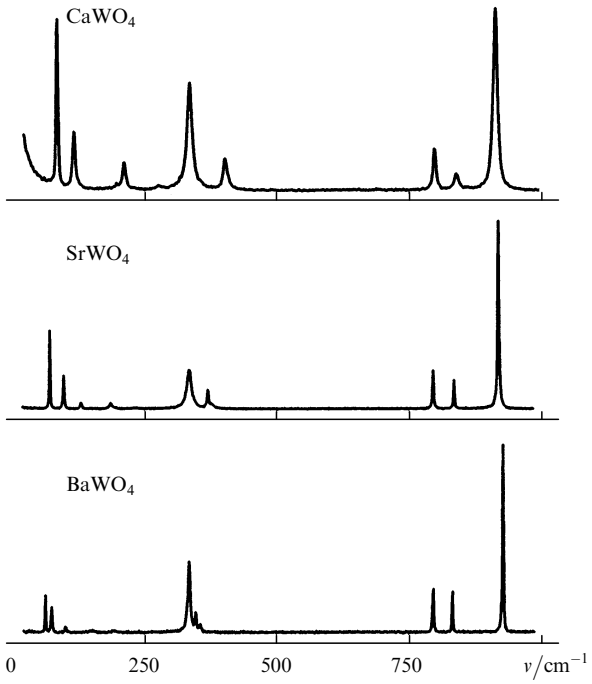

Figure 1. Spontaneous Raman spectra of alkaline-earth tungstate crystals.

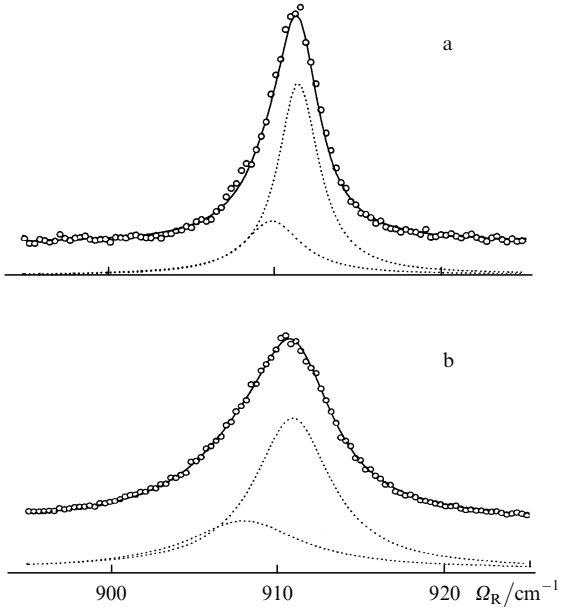

Figure 2. Spontaneous Raman spectra of the A_{1g} mode of a $CaWO_4$ crystal (○) at temperatures of 77 K (a) and 300 K (b) and the resolution of the experimental spectrum into two Lorentzian components (dotted curves).

Table 1. Spectral parameters of SRS-active lines of spontaneous Raman scattering in alkaline-earth tungstate crystals.

Crystal	Ω_R/cm^{-1}		$\Delta\Omega_R/cm^{-1}$		$\omega_{lat}^{max}/cm^{-1}$
	$T=77$ K	$T=300$ K	$T=77$ K	$T=300$ K	
$CaWO_4$	911.6	911.2	3.6	6.9	274
$CaWO_4^*$	911.4	910.8	3.0	5.6	274
$SrWO_4^{**}$	922.2	921.5	1.45	3	240
$BaWO_4$	926.5	926	0.97	1.6	194

*The data for $CaWO_4$ correspond to the strongest line in an inhomogeneously broadened spectrum, resolved into two components. **Polycrystalline sample.

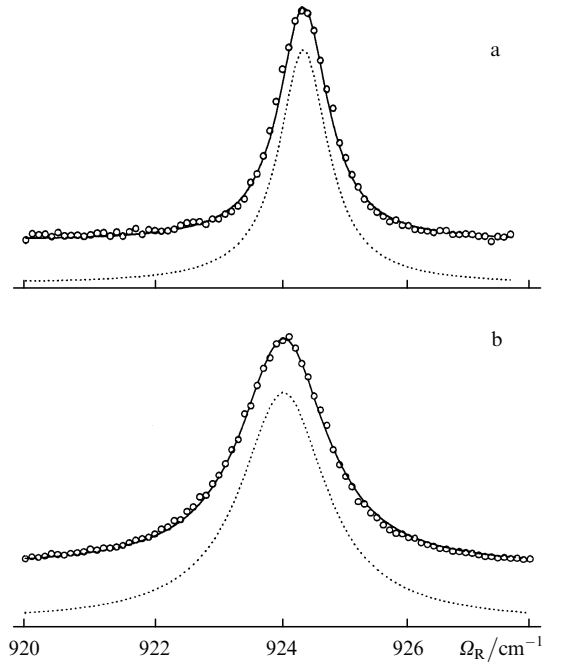

Figure 3. Spontaneous Raman spectra of the A_{1g} mode of a $BaWO_4$ crystal (○) at temperatures of 77 K (a) and 300 K (b) and the approximation of the experimental spectrum by the Lorentzian line (dotted curves).

lines with a frequency shift of about 0.8 cm^{-1}. Fig. 2 shows the spontaneous Raman spectra of the A_{1g} mode at 300 K and 77 K, recorded with a high spectral resolution, and their resolution into the two components. A study of polarised spontaneous Raman spectra showed that both components of the high-frequency line in $CaWO_4$ belong to the A_{1g} asymmetry. The splitting of the A_{1g} mode can be attributed to two types of the WO_4 tetrahedra present in the $CaWO_4$ crystals and differing slightly in structure. It is likely that this difference between the structures of the WO_4 tetrahedra is the result of a specific feature of the structure of the $CaWO_4$ crystal lattice or of the presence of defects. The asymmetry of the profile of the high-frequency line in the spontaneous Raman spectra is unrelated to the conditions used in the synthesis of the $CaWO_4$ crystals because it was observed both for the single crystals grown from the melt at $T = 1580$ °C and for the polycrystalline boules produced by sintering at a lower temperature ($T = 1100$ °C). A considerable inhomogeneous broadening of the SRS-active mode in $CaWO_4$, both at 300 K and at 77 K, is responsible for a reduction in the peak value of the Raman scattering cross section and for the resulting reduction in SRS gain.

This shortcoming is not observed for other tungstates under study, namely, $SrWO_4$ and $BaWO_4$. The spontaneous Raman spectra of A_{1g} modes in these crystals measured at 77 K and 300 K are well described by a Lorentzian curve. Fig. 3 presents the spontaneous Raman spectra of the A_{1g} mode in the $BaWO_4$ crystal at 77 K and 300 K, and their fit. As temperature is increased from 77 K to 300 K, the position of the peak of the SRS line shifts slightly to the high-frequency region and the spectral width decreases by a factor

Table 2. Parameters of SRS-active modes in crystals at $T = 300$ K.

Crystal	Spatial group of the lattice	Ω_R/cm^{-1}	$\Delta\Omega_R/cm^{-1}$	Σ_{int} (%)	Σ_{peak} (%)	Geometry of scattering excitation	
						k	***E***
Diamond	O_h^7	1332.9	2.7	100	100	$\parallel C_3$	$\perp C_3$
$Ba(NO_3)_2$	T_h^6	1048.6	0.4	21	63	$\parallel C_4$	$\parallel C_4$
$CaWO_4$	C_{4h}^6	911.2	6.9	47	18	$\perp C_4$	$\parallel C_4$
$BaWO_4$	C_{4h}^6	926	1.6	47	64	$\perp C_4$	$\parallel C_4$
$BaWO_4$	C_{4h}^6	926	1.6	38	52	$\perp C_4$	$\perp C_4$
$KGd(WO_4)_2$	C_{2h}^6	901	5.4	54	25	$\perp C_2$	$\perp C_2$
$KGd(WO_4)_2$	C_{2h}^6	768	6.4	65	29	$\perp C_2$	$\parallel C_2$

Note: The peak and integrated cross sections are given in percent relative to the cross sections for a diamond crystal; ***k*** is the wave vector; ***E*** is the electric vector of the optical field; C_2, C_3, and C_4 are the crystallographic axes.

of about two. This fact is of substantial interest because it shows that the development of a Raman laser operating at cryogenic temperatures can increase considerably the SRS gain and lower the threshold of Raman lasing in these media.

Table 2 presents the relative integrated and peak values of the scattering cross section for $CaWO_4$, $BaWO_4$, $KGd(WO_4)_2$, and $Ba(NaO_3)_2$ single crystals at 300 K. One can see that the $CaWO_4$ and $BaWO_4$ crystals have nearly the same integrated scattering cross sections Σ_{int}, but $BaWO_4$, owing to the fourfold line narrowing, is characterised by a fourfold increase of the peak value Σ_{peak} (up to 64%). This value is comparable to Σ_{peak} for the strongest line in the Raman spectra of the $Ba(NO_3)_2$ crystal (63%) and proves that the $BaWO_4$ crystal offers much promise for the study of SRS and the development of Raman lasers. Although the integrated cross section for tungstate crystals exceeds the value for the barium nitrate crystal by a factor of two or three, the peak cross sections for $CaWO_4$ and $KGd(WO_4)_2$ are several times lower because of the larger width $\Delta\Omega_R \sim 5-7$ cm^{-1}. The small width of the SRS line in the $BaWO_4$ crystal ($\Delta\Omega_R \sim 1.6$ cm^{-1}) ensures a high peak scattering cross section $\Sigma_{peak} = 63\%$. For a polycrystalline $SrWO_4$ sample, we observed a wider line in the Raman spectrum ($\Delta\Omega_R \sim 3$ cm^{-1}). Under the assumption that the integrated cross section of the A_{1g} mode in tungstate crystals is constant, one can estimate the peak cross section of $SrWO_4$, which gives $\Sigma_{peak} \sim 30\%$. This value is lower than the one for the $Ba(NO_3)_2$ crystal, but it is somewhat higher than the values for the SRS-active lines in the $KGd(WO_4)_2$ crystal. It follows that the $SrWO_4$ crystal is also promising for Raman lasers.

3. Raman lasing in the barium tungstate crystal

Measurement of the SRS threshold made it possible to determine real values of the SRS gain for different crystals and to compare them. The experimental setup is shown schematically in Fig. 4. A single-mode repetitively pulsed Nd^{3+} : YAG crystal with passive Q-switching by a LiF crystal with F_2^- colour centres was used as the pump source. Its output radiation was amplified in a single-pass amplifier up to an energy of 20 mJ. The laser pulses were 12 ns long, and their repetition frequency was 10 Hz. In experiments in the visible spectral region the radiation frequency was doubled in a KTP crystal and the output pulses reached 10 mJ in energy.

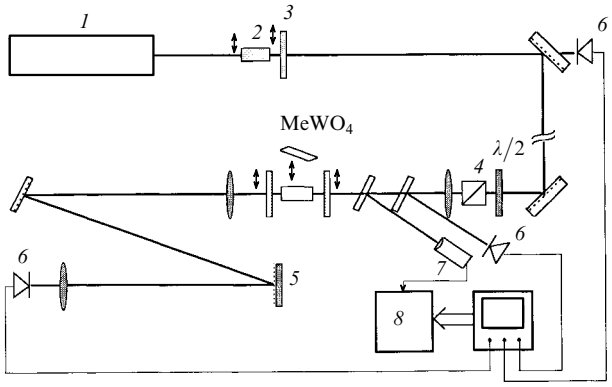

Figure 4. Experimental setup for measurement of the SRS thresholds: (*1*) Nd^{3+} : YAG laser with a passive switch; (*2*) frequency doubler; (*3*) filter; (*4*) Glan prism; (*5*) diffraction grating; (*6*) photodiodes; (*7*) CCD camera; (*8*) personal computer.

The radiation energy was smoothly varied with the aid of a phase plate and a Glan prism. The pump radiation was focused at the centre of a sample by a lens with the focal length $f = 50$ or 80 cm.

The pump beam profiles in the focal plane were monitored with the aid of a CCD camera with a pixel size of 8.6 μm. They matched well the Gaussian distributions with diameters of 90 and 170 μm at half-maximum for the lenses with $f = 50$ and 80 cm ($\lambda = 1.064$ μm) and with a diameter of 120 μm for the lenses with $f = 80$ cm ($\lambda = 0.532$ μm). A portion of the exciting radiation was reflected from a glass plate and directed to a Ge photodiode for measuring the pump energy. The Stokes radiation excited in the sample was collimated by a lens, spectrally selected by a diffraction grating, and detected with a Ge photodiode. We carried out simultaneous and independent measurements of the pump energy and the scattered Stokes radiation for separate laser pulses with the aid of a digital storage oscilloscope.

The scattering cross section and the SRS gain are known to depend on the excitation wavelength. For the $Ba(NO_3)_2$ crystal, the gain was 11 cm GW^{-1} for $\lambda = 1.064$ μm and 47 cm GW^{-1} for $\lambda = 0.532$ μm [7, 8]. As a result, a high radiation power is needed to reach the SRS threshold in the near-IR region. Our initial experiments were made at the wavelength of 1.064 μm.

At pump powers below the optical breakdown, the SRS threshold was reached in short crystals by placing them in a cavity 9 cm long, which was formed by two plane dielectric mirrors. The input mirror had $R_{1.064} < 5\%$ and $R_{1.1-1.25} > 98\%$, and the output mirror had $R_{1-1.2} \sim 55\%$. As shown earlier [9], the use of an additional cavity for an SRS crystal makes it possible to lower the SRS threshold energy and this energy remains inversely proportional to the crystal length. This is also true of the SRS gain.

Fig. 5 and Table 3 present the experimental dependences of the SRS lasing efficiency η on the pump energy W_p and the threshold pump energies W_p^{th} for the $BaWO_4$ (with length $L = 31$ mm), $KGd(WO_4)_2$ (36 mm), and $Ba(NO_3)_2$ (25 mm) crystals when the pump radiation was focused by the lens with $f = 50$ cm. One can see that the threshold pump energy for SRS in the $KGd(WO_4)_2$ crystal exceeded the value for the barium tungstate and nitrate crystals by a factor of about two, even though $KGd(WO_4)_2$ was somewhat longer.

Table 3 also gives the values of the SRS gain G calculated for the materials studied. They were obtained under the assumption that the $Ba(NO_3)_2$ crystal has a gain $G = 11$ cm GW^{-1}. One can see that the $BaWO_4$ and $Ba(NO_3)_2$ crystals have similar values of the SRS gain. It was impossible to carry out an absolute calculation of the SRS gain from these experiments because a correct allowance for the cavity effects associated with reflection from the mirrors and crystal faces is a complicated problem. It is likely that the difference between the SRS gain for the $KGd(WO_4)_2$ crystal (36 mm) and the value given in the literature is associated with the following fact. If the pump radiation is focused by the lens with $f = 50$ cm, the crystal length becomes comparable with the beam-waist length and one cannot use the model of a uniform pump distribution throughout the crystal length.

It is clear from Fig. 5 that the real efficiency of SRS conversion of the radiation with $\lambda = 1.064$ μm reaches 26% in the $Ba(NO_3)_2$ crystal and 20% in $BaWO_4$. In the experiments with $BaWO_4$, we did not reach saturation of conversion with increasing pump power, and it is reasonable to expect a further increase in the degree of conversion. The differential efficiencies of SRS lasing in the barium tungstate and nitrate crystals were greater than 75%, which promises a further increase in the real efficiency through optimisation of the pumping conditions and of the external SRS cavity.

The external cavity and the reflection from the crystal faces have a strong effect on the accuracy with which the SRS threshold is measured, and they noticeably reduce its value. To eliminate this effect in the threshold measurements, we prepared $Ba(NO_3)_2$ (40 mm) and $BaWO_4$ (25 mm) crystals with the Brewster faces. To reach the SRS threshold without a cavity, we used pumping by the second harmonic of the Nd^{3+} : YAG laser. Fig. 6 gives the dependences of the Stokes component on the pump energy for the focusing lens with $f = 80$ cm. Table 4 presents the threshold pump energies W_p^{th}. One can see that the plane-parallel sample had a lower SRS threshold, attributed to the influence of the cavity effects associated with the crystal faces. In the Brewster samples, the SRS threshold was observed at an

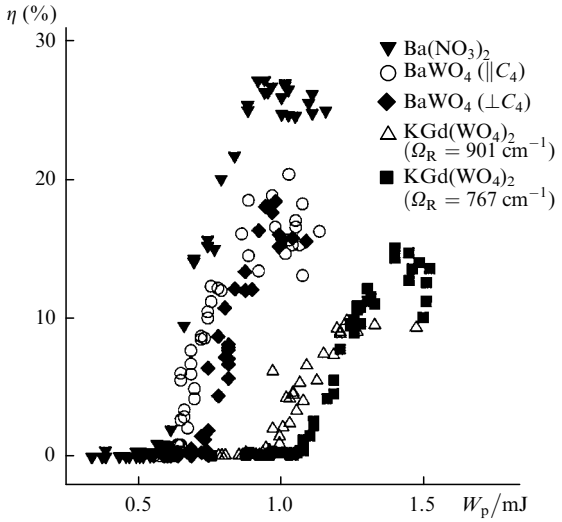

Figure 5. Dependences of the Stokes lasing efficiency η on the energy W_p of pump radiation with $\lambda = 1.064$ μm focused by a lens with $f = 50$ cm into the $Ba(NO_3)_2$ ($L = 25$ mm), $BaWO_4$ (31 mm), and $KGd(WO_4)_2$ (36 mm) crystals placed in the cavity.

Table 3. Threshold energy for SRS in the crystals under study, placed in the external cavity and pumped by radiation with $\lambda = 1.064$ μm focused into the crystals by the lens with $f = 50$ cm.

Crystal	L/mm	Ω_R/cm^{-1}	W_p^{th}/mJ	G^*/cm GW^{-1}
$BaWO_4$ (∥C_4)	31	925	0.65	8.5
$BaWO_4$ (⊥ C_4)	31	925	0.76	7.2
$Ba(NO_3)_2$	25	1047	0.65	11
$KGd(WO_4)_2$	36	901	0.98	4.8
$KGd(WO_4)_2$	26	767	1.08	4.4

*The SRS gain G was calculated on the assumption that its value for the $Ba(NO_3)_2$ crystal is 11 cm GW^{-1} [8].

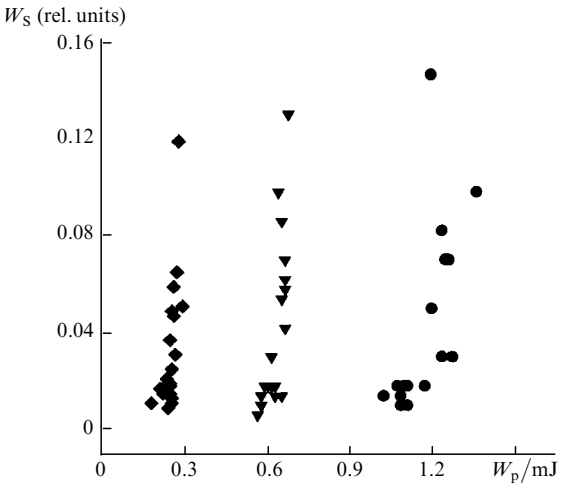

Figure 6. Dependences of the Stokes component energy W_S on the pump energy W_p ($\lambda = 0.532$ μm) for the pump radiation focused by a lens with $f = 80$ cm in the Brewster $Ba(NO_3)_2$ ($L = 40$ mm, ▼) and $BaWO_4$ (25 mm, ●) crystals and the plane-parallel $BaWO_4$ crystal (31 mm, ◆).

Table 4. Parameters of SRS in Brewster $Ba(NO_3)_2$ and $BaWO_4$ crystals (without an external cavity) for single-pass excitation by $\lambda = 0.532$ μm radiation focused by a lens with $f = 80$ cm.

Crystal	L/mm	W_p^{th}/mJ	G/cm GW^{-1}
$Ba(NO_3)_2$	40	0.65	52
$BaWO_4$	25	1.20	36

energy of 0.65 mJ for $Ba(NO_3)_2$ and at 1.20 mJ for $BaWO_4$. We used the real spatial and time distributions of the pump energy in this experiment and calculated the SRS parameters for the single-pass amplification in the absence of reflections. The SRS gain was found to be 36 cm GW^{-1} for $BaWO_4$ and 52 cm GW^{-1} for $Ba(NO_3)_2$. The accuracy of its determination, limited by fluctuations of the spatial and time distributions of the pump energy, was about 20%.

Our study supports the aforementioned assumption that the $BaWO_4$ crystal offers promise for the use in SRS. We emphasise that this crystal, in addition to a high peak cross section Σ_{peak}, close to the value for $Ba(NO_3)_2$, has a high integrated scattering cross section Σ_{int}, typical of other tungstate crystals as well. It is thus expected that the $BaWO_4$ crystal will provide a high efficiency for the SRS conversion not only of nanosecond laser pulses, but also of subnanosecond and picosecond pulses as well.

4. Conclusions

Our study of the alkaline-earth tungstate crystals by means of spontaneous Raman spectroscopy made it possible to predict and confirm that the new barium and strontium tungstate crystals show promise for their use in SRS converters, Raman lasers, and Raman amplifiers. In the laser experiments on the SRS threshold, the SRS gain for barium tungstate was found to be 36 cm GW^{-1} (for $\lambda = 0.532$ μm), which is only 20% lower than the value for barium nitrate characterised by the highest efficiency among SRS materials. In contrast to $Ba(NO_3)_2$, the $BaWO_4$ crystal is nonhygroscopic and has a high thermal conductivity and hardness, which enhances the potential of its use in Raman lasers and substantially simplifies their operating conditions.

Acknowledgements. This work was partially supported by the European Agency of Aerospace Research, the Agency of Scientific Research, the Research Laboratory of the United States Air Force (Contract No. F61775-99-WE024), the Russian Foundation for Basic Research (Grant No. 98-02-16523), CRDF (USA), and the Ministry of Science of the Russian Federation (Grant No. RP-2-514).

References

1. Eckhardt G *IEEE J. Quantum Electron.* **2** 2 (1996)
2. Ivanyuk A M, Ter-Pogosyan M A, Shaverdov P A, Belyaev V D, Ermolaev V L, Tikhonov N P *Opt. Spektrosk.* **59** 950 (1985) [*Opt. Spectrosc. (USSR)* **59** 572 (1985)]
3. Andryunas K, Vishchakas Yu, Kabelka V, Mochalov I V, Pavlyuk A A, Petrovskiĭ G T, Syrus V *Pis'ma Zh. Eksp. Teor. Fiz.* **42** 333 (1985) [*JETP Lett.* **42** 410 (1985)]
4. Zverev P G, Basiev T T, Osiko V V, Kulkov A M, Voitsekhovskiĭ V N, Yakobson V E *Opt. Mater.* **11** 315 (1999)
5. Berenberg V A, Karpukhin S N, Mochalov I V *Kvantovaya Elektron. (Moscow)* **14** 1849 (1987) [*Quantum Electron.* **17** 1178 (1987)]
6. Basiev T T, Sobol A A, Zverev P G, Osiko V V, Powell R C *Appl. Opt.* **38** 594 (1999)
7. Eremenko A S, Karpukhin S N, Stepanov A I *Kvantovaya Electron. (Moscow)* **7** 196 (1980) [*Quantum Electron.* **10** 113 (1980)]
8. Basiev T T, Voĭtsekhovskiĭ V N, Zverev P G, Karpushko F V, Lyubimov A V, Mirov S B, Morozov V P, Mochalov I V, Pavlyuk A A, Sinitsyn G V, Yuakobson V É *Kvantovaya Elektron. (Moscow)* **14** 2452 (1987) [*Quantum Electron.* **17** 1560 (1987)]
9. Zverev P G, Basiev T T, Prokhorov A M *Opt. Mater.* **11** 335 (1999)